Int J Adv Manuf Technol (2017) 92:3385–3397
DOI 10.1007/s00170-017-0400-4

ORIGINAL ARTICLE

Gas compensation-based abrasive flow processing method for complex titanium alloy surfaces

Li Zhang[1] · **Jin-shun Wang**[1] · **Da-peng Tan**[1,2] · **Zhi-min Yuan**[1]

Received: 3 October 2016 / Accepted: 3 April 2017 / Published online: 24 April 2017

Abstract To resolve the problems of uniformity and efficiency of soft abrasive flow (SAF) processing for complex titanium alloy surfaces, a gas compensation-based abrasive flow (GCAF) processing method is proposed. By the constrained modules, an enclosed flow passage covering the titanium alloy surface is built up, in which the gas phase is injected to enhance the turbulence intensity of abrasive flow. Taking the constrained flow passage as the objective, a three-phase fluid mechanic model for GCAF is set up based on the realizable k-ε model and the mixture model. The profiles of velocity and dynamical pressure of abrasive flow field in the constrained flow passage are obtained, and the turbulence variation regulars caused by gas compensation are revealed. Numerical results show that the proposed method can strengthen the turbulence intensity of abrasive and improve the distribution uniformity of dynamical pressure. A GCAF processing experimental platform is developed, and the experiments are performed. The results prove that the proposed method can obtain better processing efficiency and uniformity, the average surface roughness is less than Ra 0.3, and the surface topograph of micro-peak and micro-valley can reach less than 50 and 10 μm, respectively.

Keywords Gas compensation-based abrasive flow (GCAF) · Titanium alloy surfaces · Constrained flow passage · Turbulence intensity

✉ Da-peng Tan
tandapeng@zjut.edu.cn

[1] Key Laboratory of E&M, Ministry of Education and Zhejiang Province, Zhejiang University of Technology, Hangzhou 310014, China

[2] State Key Lab of Digital Manufacturing Equipment and Technology, Wuhan 430074, China

1 Introduction

Titanium alloy materials possess perfect mechanic performances, such as low density (4.5 g/cm^3), good corrosion resistance, and biocompatibility [1–4], so they have been applied in many engineering areas, especially for the artificial joints manufacturing. The technical procedures of titanium artificial joints contain casting, forging, hot static pressing, and machining. The surface quality of artificial joints determines the surface friction properties. As the artificial organs, they cannot be directly applied for implantation without finishing; otherwise, the higher roughness might increase the contact probabilities between the joint surfaces and micro-convex bodies and result in larger adhesion wear [5, 6].

Generally, the artificial joints have the body surfaces with complex or irregular geometric shape (shown in Fig. 1); thereby, traditional mechanical processing methods are hard to satisfy the technical requirements [7, 8]. Moreover, the titanium alloy materials have higher visco-elasticities and lower heat conductivities, so the abrasive flow machining (AFM) methods are apt to create surface scratches and heat damages [9, 10]. To resolve the problems, the soft abrasive flow (SAF) processing method is proposed [11–13]. It uses one or several mechanical constrained modules to cover the joint surface and constructs an enclosed re-circulating flow passage. The fluid medium has lower viscosity, particle faction, and higher velocity, so it has better flow performance. Therefore, SAF is easy to generate the turbulent flow state, which can improve the surface quality and adapt the complex geometric surfaces of artificial joints.

Owing to the technical advantages of SAF processing method, it has been widely applied in the mechanical manufacturing area including micro-electro-mechanical components, precise molds, and automobile accessories [14–16]. In 2010, Ji et al. used the Newton multiple-phase method to describe the SAF flow field in constrained flow passage and

Fig. 1 Titanium alloy artificial joints with complex geometric surfaces

obtained the motion trails of abrasive particles in the near-wall region by discrete phase model (DPM) [10]. In 2012, Tan et al. proposed a level set method (LSM) based fluid mechanic modeling method for SAF processing and adopted the higher-order essentially non-oscillatory (ENO) and total variation diminishing (TVD) methods to reveal the dynamical variation regulars of phase surface of two-phase abrasive flow [17]. Li et al. presented a two-phase fluid mechanic model for SAF near-wall region. The profiles of SAF turbulent energy, velocity, and dynamical pressure with different boundary conditions were obtained by the semi-implicit method for pressure-linked equation consistent (SIMPLEC) algorithm. The processing experiment for a micro U-shape workpiece proved that SAF method could improve the processing precision of irregular geometric surfaces [4]. In 2014, Ji et al. put forward a SAF finishing method based on ultrasound enhancing. The particle image velocimetry (PIV) observation results showed that there are large numbers of bubbles that were growing and hitting on the wall continuously, which could lead to positive effects for the processing efficiency [18]. In 2015, Zhang et al. used the SAF to process titanium alloy artificial joints, and then found that fluid resistance caused path losses, local losses, and uneven profiles of velocity and dynamic pressure of abrasive flow field. Those ultimately result in uneven processing effects and lower efficiency [19]. In 2016, Tan et al. introduced the fluid collision theory into fluid-based processing area and proposed a double-inlet SAF finishing method. The processing experiments show that the proposed SAF finishing method can make the roughness on parallel flowing direction be less than 50 nm and can improve the finishing uniformity and efficiency [20]. Ji et al. proposed a gas-liquid-solid three-phase abrasive flow finishing method. By introducing micro-nano gas into a SAF field, the method utilized the energy released by the gas collapsing to accelerate the motions of abrasive particles and to improve the processing efficiency [21].

From the above references, it can be inferred that SAF processing has the problem of low processing efficiency and apt to form uneven surface quality in the larger curvature region or static flow corner. For the special processing characteristics of titanium alloy, the above problems might become apparent. Consequently, to address the matter, we propose a gas compensation-based abrasive flow (GCAF) processing method, in which the gas is drove to the constrained passage at a suitable combination of compensation velocity, compensation area, and incident angle.

Apparently, different from the traditional SAF and other fluid-based processing methods, GCAF is with the three-phase fluid medium. The gas phase is injected into the constrained flow passage by several inlets, disturbs the flow field distribution, and avoids the processing dead regions. Moreover, the energy of gas phase can enhance the turbulence intensity of SAF, and the collision probabilities between abrasive particles and workpiece surface would be increased.

This paper is organized as follows. In Sect. 2, a three-phase fluid mechanic model of GCAF is set up based on the realizable k-ε model and the mixture model. In Sect. 3, the physical boundary conditions of the constrained flow passage are described, the numerical simulations for the flow field characteristics of the constrained passages are performed, and the comparison analysis and discussion are given. In Sect. 4, a GCAF finishing experimental platform is developed, and the experiments are implemented. In Sect. 5, the conclusions are presented.

2 Fluid mechanic model of GCAF

2.1 Turbulence model

As indicated in Sect. 1, GCAF has the similar physical characters with SAF, i.e., low viscosity and high flow velocity, so it easily develops into turbulent flow state. As a classical turbulence model, the standard k-ε model is one of the most widely used models, but it may have nonphysical results caused by high mean shear stress. Moreover, considering the modeling of strong swirl flow, curved wall flow, or streamline flow, it can lead to flow stress distortion or negative normal stress [22]. For above reasons, the realizable k-ε model is proposed [23], where the rotation speed and correlated variables of curvature are considered in the model function.

Therefore, it has a better computation performance on the flow fields with strong streamline curvature, vortex, and rotation.

The turbulent kinetic energy and its dissipation rate transport equation of realizable k-ε can be described as

$$\frac{\partial(\rho k)}{\partial t}+\frac{\partial(\rho k u_i)}{\partial x_i}=\frac{\partial}{\partial x_j}\left[\left(\mu+\frac{\mu_t}{\sigma_k}\right)\frac{\partial_k}{\partial x_j}\right]+G_k-\rho\varepsilon \tag{1}$$

$$\frac{\partial(\rho\varepsilon)}{\partial t}+\frac{\partial(\rho\varepsilon u_i)}{\partial x_i}=\frac{\partial}{\partial x_j}\left[\left(\mu+\frac{\mu_t}{\sigma_\varepsilon}\right)\frac{\partial_\varepsilon}{\partial x_j}\right]+\rho C_1 E\varepsilon-\rho C_2\frac{\varepsilon^2}{k+\sqrt{\nu\varepsilon}} \tag{2}$$

where k represents the turbulent kinetic energy, u_i represents the fluid velocity, $G_k=\mu_t\left(\frac{\partial u_i}{\partial x_j}+\frac{\partial u_j}{\partial x_i}\right)\frac{\partial u_i}{\partial x_j}$ is caused by turbulent kinetic energy, σ_k is the Prandtl number of turbulent kinetic energy caused by mean velocity gradient, σ_ε is the Prandtl number of turbulent kinetic energy dissipation rate, E represents the modulus of time-averaged strain rate tensor, $C_2=1.9$, $C_1=Max\left(0.43,\frac{\eta}{\eta+5}\right)$ is the coefficient, $\eta=\left(2E_{ij}\cdot E_{ij}\right)^{1/2}\frac{k}{\varepsilon}$ is the intermediate variable, and $E_{ij}=\frac{1}{2}\left(\frac{\partial u_i}{\partial x_j}+\frac{\partial u_j}{\partial x_i}\right)$ is the modulus of time-averaged strain rate tensor.

The turbulent viscosity μ_t is the key parameter for turbulence computation. Different from other turbulence models, realizable k-ε model regards μ_t as a variable:

$$\mu_t=\rho C_\mu\frac{k^2}{\varepsilon} \tag{3}$$

$$C_\mu=\frac{1}{4+\sqrt{6}\cos\varphi U^* k/\varepsilon} \tag{4}$$

$$W=\frac{E_{ij}E_{jk}E_{kj}}{\left(E_{ij}E_{ij}\right)^{1/2}} \tag{5}$$

$$U^*=\sqrt{E_{ij}E_{ij}+\tilde{\Omega}_{ij}\tilde{\Omega}_{ij}} \tag{6}$$

where Ω_{ij} is the time-averaged strain rate tensor, $\tilde{\Omega}_{ij}=\Omega_{ij}-2\varepsilon_{ijk}\omega_k$, $\Omega_{ij}=\overline{\Omega}_{ij}-\varepsilon_{ijk}\omega_k$, and ω_k is the angular velocity [24–26].

According to the Eqs. 3–6, it is found that C_μ is a key variable of μ_t, and it can be regarded as function containing the parameters of rotating velocity, time-averaged strain, turbulent parameters, and angular velocity. In view of the above character, realizable k-ε model has the ability to simulate the flow field profiles of boundary layer fluid [27, 28]. Therefore, it can obtain more accurate Reynolds stress than the standard k-ε model or renormalization group (RNG) k-ε model and accords with the factual physical features of turbulent flow, adapting for multi-phase flow, jet flow, and shear flow. Accordingly, the above merits can offer adequate theoretical references to the research works of boundary layer division and two-phase interface coupling involved by the GCAF modeling.

2.2 Multiphase flow model

As indicated in Sect. 1, the research objective of the paper is the three-phase abrasive flow in a limited physical space, and it should be described by a multiphase flow model. Presently, volume of fluid (VOF) model and mixture model are the most commonly used models for multiphase flow. The mixture model can simulate the multiphase flow fields with two or more phases at different velocities. It can solve the momentum equation and describe the discrete phase by relative velocity. Furthermore, the mixture model allows the penetration of each phase; so, it can accurately simulate the abrasive flow under unclear drag force regular [29–32]. Because the velocity of gas is different from that of the SAF, and all phases in the constrained passage are mixed with each other during the processing, the mixture model is more consistent with the actual case of the GCAF.

The momentum equation of the mixture model can be obtained by the individual momentum equation and can be described as follows:

$$\frac{\partial}{\partial_t}\left(\rho_m\vec{\nu}_m\right)+\nabla\cdot\left(\rho_m\vec{\nu}_m\vec{\nu}_m\right)=-\nabla p+\nabla\cdot\left[\mu_m\left(\nabla\vec{\nu}_m+\nabla\vec{\nu}_m^{\,T}\right)\right]+\rho_m\vec{g}+\vec{F}+\nabla\cdot\left(\sum_{k=1}^{n}\partial_k\rho_k\vec{\nu}_{dr,k}\vec{\nu}_{dr,k}\right) \tag{7}$$

where m represents the mixture fluid mass, $\rho_m=\sum_{k=1}^{n}\alpha_k\rho_k$ represents the mixture fluid density, α_k means the volume fraction of k phase, ρ_k is the density of k phase, $\vec{\nu}_m=\frac{\sum_{k=1}^{n}\alpha_k\rho_k\vec{\nu}_k}{\rho_m}$ is the average velocity of mixed phase, $\vec{\nu}_k$ is the average velocity of k phase, p is the mixture fluid pressure, $\mu_m=\sum_{k=1}^{n}\partial_k\mu_k$ is the coefficient of viscosity of mixed phase, μ_k is the coefficient of viscosity of k phase, $\vec{g}$ is the gravity, $\vec{\nu}_{dr,k}=\vec{\nu}_k-\vec{\nu}_m$ is the drift velocity of k phase, n represents the phase number, and $\nabla=\frac{\partial}{\partial x}i+\frac{\partial}{\partial y}j+\frac{\partial}{\partial z}k$ is the Hamilton operator [33–35].

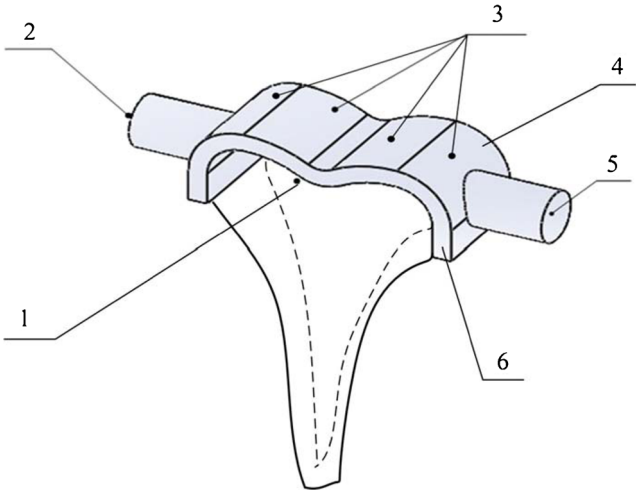

Fig. 2 Constrained flow passage model of the GCAF processing method: *1* workpiece (joint) surface, *2* passage inlet (two-phase abrasive flow), *3* gas inlets, *4* constrained module, *5* passage outlet (three-phase abrasive flow), *6* constrained flow passage

Based on the above hypothesis, the energy equation of the mixture model can be described as follows:

$$\frac{\partial}{\partial_t}\left(\sum_{k=1}^{n}\alpha_k\rho_k E_k\right)+\nabla\cdot\sum_{k=1}^{n}\left(\alpha_k\vec{\nu}_k(\rho_k E_k+p)\right)=\nabla\cdot\left[k_{eff}\nabla T\right]+S_E \tag{8}$$

where $E_k = h_k$ represents the energy of k phase, h_k represents the sensible enthalpy of k phase, k_{eff} represents the effective conduction rate, T represents the temperature of mixture fluid, and S_E represents the heat sources.

3 Numerical simulations

3.1 Objective and its boundary conditions

For the constrained flow passage of the proposed GCAF processing method, a fluid mechanic model is set up, as shown in Fig. 2. Taking the thigh-bone joint as an instance, an enclosed constrained flow passage is constructed by eight pieces of constrained modules, which can completely cover the external surface of the joint.

The two-phase abrasive flow enters from the passage inlet, and the gas phase is injected into the flow passage by four gas inlets, with different velocities, compensation areas, or incidence angles. Then, the fluid medium becomes the three-phase abrasive flow and flows out from the passage outlet. Actually, the gas phase brings forward new energy component for fluid medium, the interactions between the abrasive flow and wall are enhanced, and the motion distortion of the abrasive flow will be strengthened.

Grid meshing directly influences the precision and effectiveness of the numerical simulation, so it is performed by the spatial discretization method. Based on the above operation, a mesh encryption method is adopted for the iterations of velocity and pressure [36]. Since pressure does not always transform laminar flow into turbulent flow, which is related to the velocity, all the inlets choose the velocity inlet, and the outlet uses the outflow. Moreover, referring to the gas injection points, the constrained passage can be divided into three segments: front, intermediate, and back, as shown in Fig. 3.

3.2 Numerical instances and result discussion

Numerical analysis of multiple-phase flow field in constrained passage can offer useful references to the technical optimization of GCAF processing. To address the issue, four numerical instances about different velocities, compensation areas, and incidence angles are provided, and the corresponding simulation parameters are listed in Table 1.

(1) Velocity profiles for different gas inlet velocities

As a fundamental flow field parameter, velocity vector can directly reflect the motion regulars of abrasive flow in the constrained flow passage. Under the conditions of incidence angle 90° and 2# gas inlet global area, the velocity profiles for different gas inlet velocities are obtained, as shown in Fig. 4.

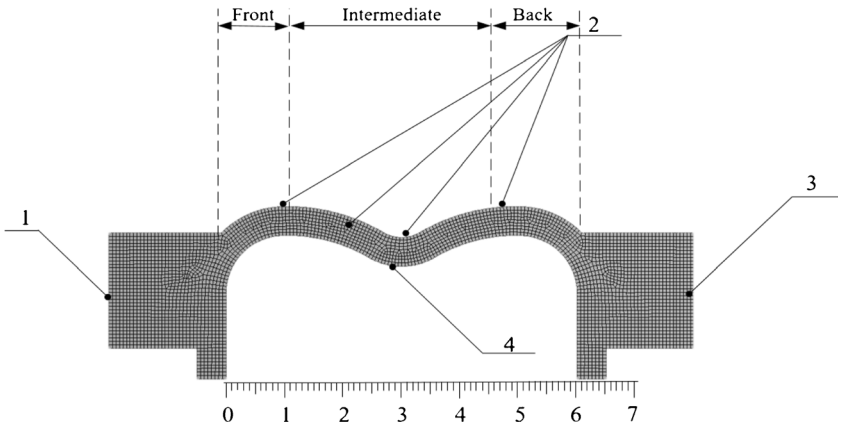

Fig. 3 Grid meshing for the constrained flow passage: *1* velocity inlet for two-phase abrasive flow, *2* velocity inlets for gas phase, *3* passage outlet for three-phase abrasive flow, *4* wall for workpiece surface

Table 1 Parameters of numerical instances

Parameters	Values
Gas inlet hydraulic diameter D/(mm)	54
Gas inlet velocity V_g/(m/s)	0, 5, 7.5, 10, 12.5
Gas compensation area	front, intermediate, back
Gas incidence angle θ/(°)	115°, 90°, 68°, 45°, 23°, 0°
Two-phase abrasive flow inlet velocity V_f/(m/s)	20
Abrasive particle fraction ϕ_B (%)	10

From the figure, we can find that the velocity profiles take on apparent uneven distributions in constrained passage, and the low-pressure regions appear on the area with larger curvature. The injection of gas phase can increase the velocity amplitude of abrasive, especially for the posterior area of gas injecting point, and can eliminate the low-pressure regions, which can cause positive effects for the processing uniformity. With the increment of gas inlet velocity, a high-velocity region is generated on the near-upper-wall area.

Since the near-wall flow field is the key region of GCAF simulation, the detailed velocity data near the workpiece surface along the fluid flow direction is obtained, as shown in the Fig. 5. Because the hydraulic diameter of passage inlet is larger than that of constrained flow passage, the velocities of GCAF are all low in the passage inlet. GCAF being entered the constrained passage, the velocities become larger, and with two times of magnitude of inlet velocities. The velocity profiles without gas compensation are with apparent fluctuation phenomena, which is caused by the water-head losing and resistance backflow. On the contrary, because of the energy supplement and flow disturbance, the velocity profiles with gas compensation have smaller variation ranges, and with higher amplitudes. Moreover, the velocity curves are varied by the shape of constrained flow passage, and it is proven that GCAF can approximate the surface of artificial joint because of the better flow motion performance.

(2) Dynamic pressure profiles for different gas inlet velocities

Dynamic pressure is converted from kinetic energy, which is the key parameter of Preston equation, and can characterize the material removing process. Considering the matter, the profiles of dynamical pressure in constrained passage are acquired, as shown in Fig. 6. Under the condition of gas compensation, the pressure profile takes on uneven distribution, especially at the vicinities of passage inlet, bottom concave, and passage outlet. Apparently, the gas compensation makes dynamical pressures near the workpiece surface tend to be uniform with the increment of constrained passage depth and with maximum value at the end of constrained passage.

With respect to the near-wall flow field, the detailed dynamical pressure data near the workpiece surface along the fluid flow direction is obtained, as shown in the Fig. 7. Under the condition of no gas compensation, the pressure profile is with uneven distribution and takes on apparent pressure shock phenomenon at the region with larger curvature. When the gas velocity is less than 5 m/s, the non-uniformity of profiles of dynamical pressure never change in front of bottom concave. However, when gas velocity is 10 m/s, dynamical pressure is divided into three areas that are the vicinity of bottom concave, the front and back of minimum concave. If the gas velocity is larger than 10 m/s, the dynamical pressure gradually expands and jumps at the end of constrained passage. Form the above phenomena, we can find that the gas compensation cannot increase the pressure amplitude but can improve the distribution uniformity of dynamical pressure.

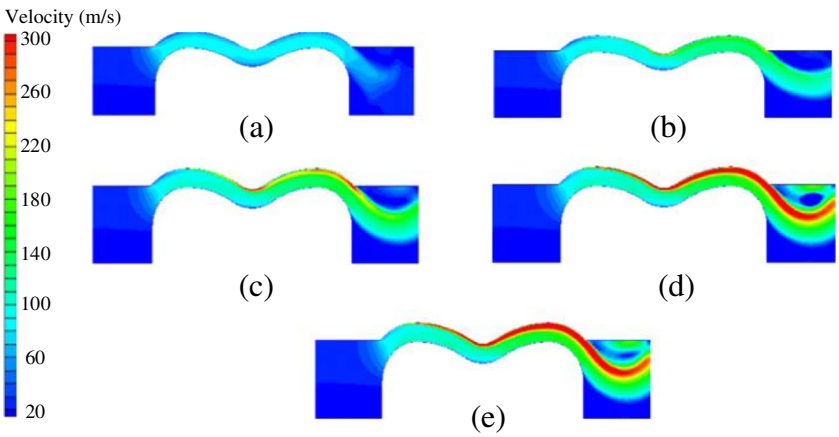

Fig. 4 Velocity profiles of GCAF in constrained passage about different gas inlet velocities: **a** 0 m/s, **b** 5 m/s, **c** 8 m/s, **d** 10 m/s, **e** 12.5 m/s

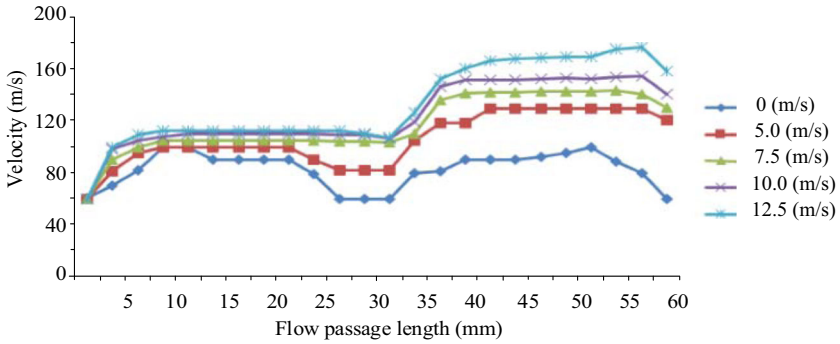

Fig. 5 Near-wall velocity curves at different gas compensation velocities

It is impossible for gas entirely mixed with abrasive flow due to hydraulic resistance. From the Fig. 8, it is seen that the gas volume forms three areas in the constrained passage. The first area close to gas inlet which appears dark red can be defined as gas concentrating area, because of its maximum gas volume fraction. The above phenomenon proves that the gas radial movement is blocked, and the transverse velocities increase rapidly by movement resistance when air enters the constrained passage. The second area that appears green at bottom of the gas concentrating area is defined as the mixture area, because the gas volume is about 0.5. The third blue area appears near the workpiece surface, in which the gas volume is less than 0.1. The thicknesses of gas concentrating area and mixing area become larger with gas velocity increment. Especially, the thickness of two areas in back of bottommost concave increases more quickly than that in front of bottommost concave. When the gas velocity is 12 m/s, the thickness of GCAF shrinks to a narrow slit which might lead to abrasive flow drying up at the end of channel.

Apparently, the gas compensation can generate effective regulation effects on velocity and dynamical pressure in the front and back bottom concave of the constrained passage. It suggests that the uneven profiles of velocity and dynamical pressure of GCAF can be compensated, due to the SAF squeezed and permeated by gas phase.

(3) Profiles of velocity and dynamical pressure for different gas compensation areas

The selection of gas phase injection points is of important influence to the compensation effects. In order to analyze the flow field characteristics about different gas compensation areas, the corresponding profiles of velocity and dynamical pressure are shown in Figs. 9 and 10, in which the compensation areas are divided into three schemes: global (front-intermediate-back) area, front-intermediate area, front area; the incidence angle of gas injection is 90°; the velocity of gas inlet is 10 m/s.

From the figures, the following regulars can be obtained. The variation of gas injection points can cause apparent velocity differences, while the changes of dynamic pressure profiles seem less remarkable. The global gas compensation scheme can obtain the most uniform flow field profiles, especially for the intermediate-back segment of the constrained flow passage. Therefore, if the flow direction of GCAF is changed, the surface quality of total workpiece surface would be guaranteed.

(4) Profiles of velocity and dynamical pressure for different incidence angles

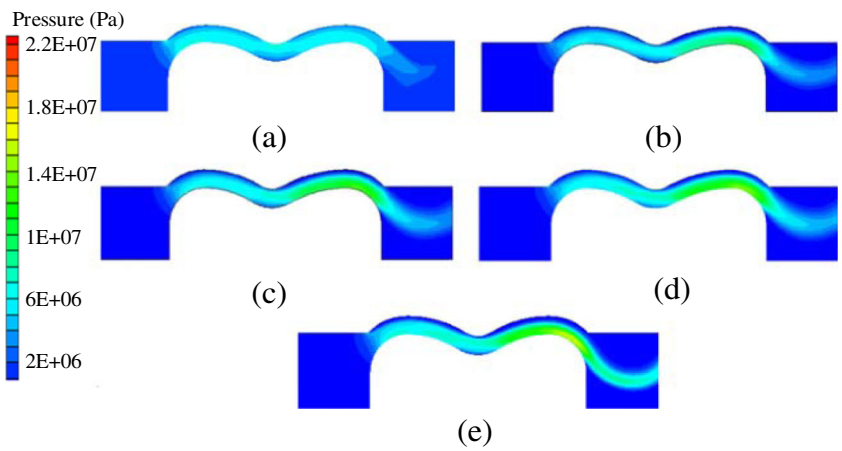

Fig. 6 Dynamical pressure profiles of GCAF in constrained passage about different gas inlet velocities: **a** 0 m/s, **b** 5 m/s, **c** 8 m/s, **d** 10 m/s, **e** 12.5 m/s

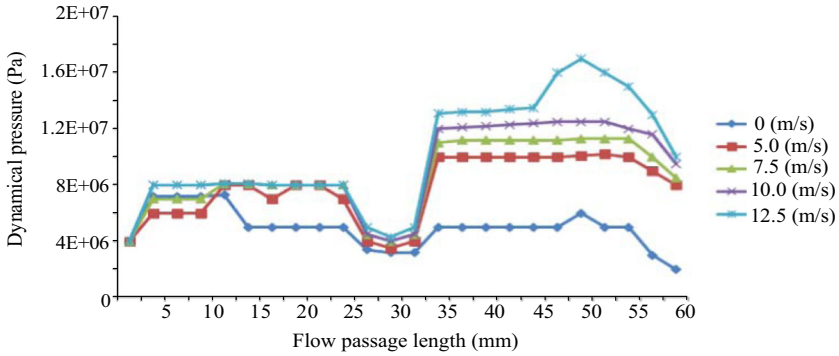

Fig. 7 Near-wall dynamical pressure curves at different gas compensation velocities

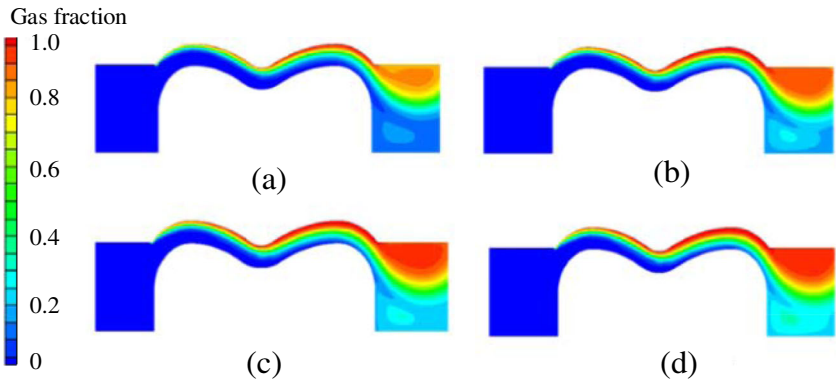

Fig. 8 The profiles of gas volume fraction of GCAF: **a** 5 m/s, **b** 8 m/s, **c** 10 m/s, **d** 12.5 m/s

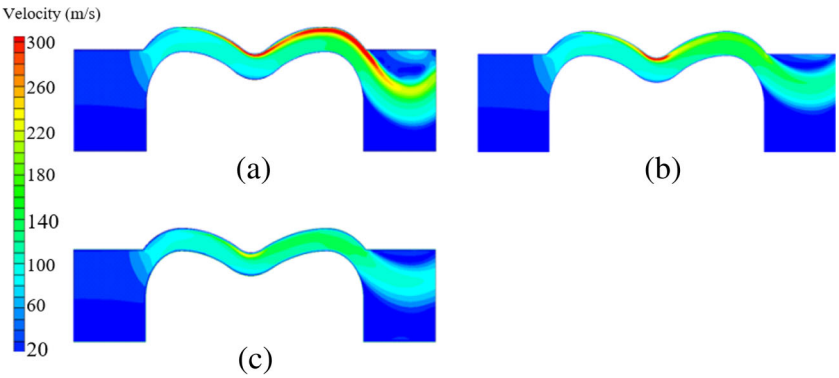

Fig. 9 Velocity profiles about different gas compensation areas: **a** global (front-intermediate-back) area, **b** front-intermediate area, **c** front area

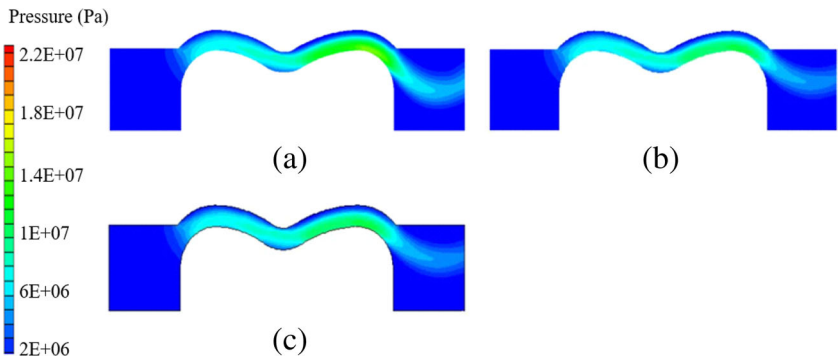

Fig. 10 Dynamic pressure profiles about different gas compensation areas: **a** global (front-intermediate-back) area, **b** front-intermediate area, **c** front area

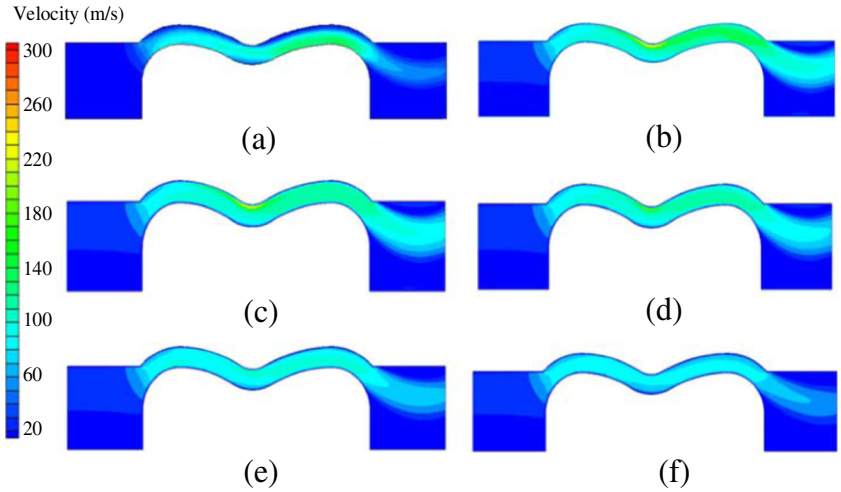

Fig. 11 Velocity profiles about different gas compensation incidence angles: **a** 115°, **b** 90°, **c** 68°, **d** 45°, **e** 23°, **f** 0°

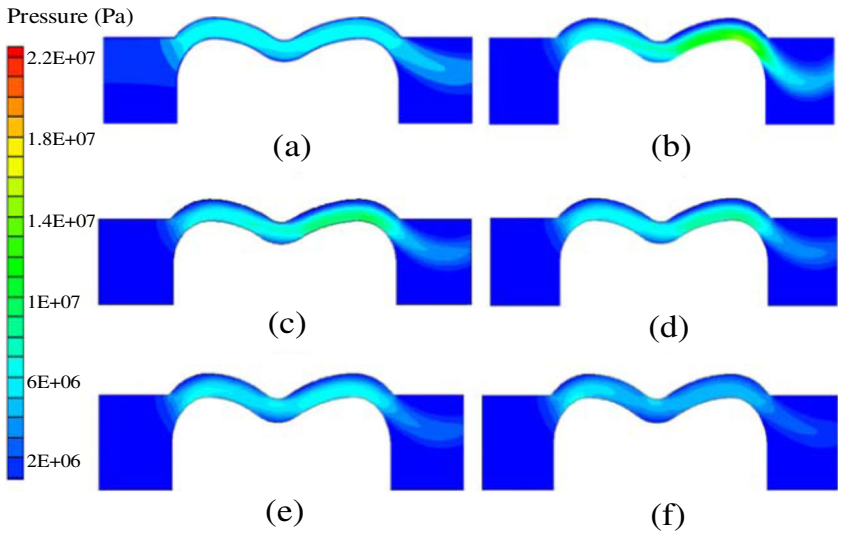

Fig. 12 Dynamical pressure profiles about different gas compensation incidence angles: **a** 115°, **b** 90°, **c** 68°, **d** 45°, **e** 23°, **f** 0°

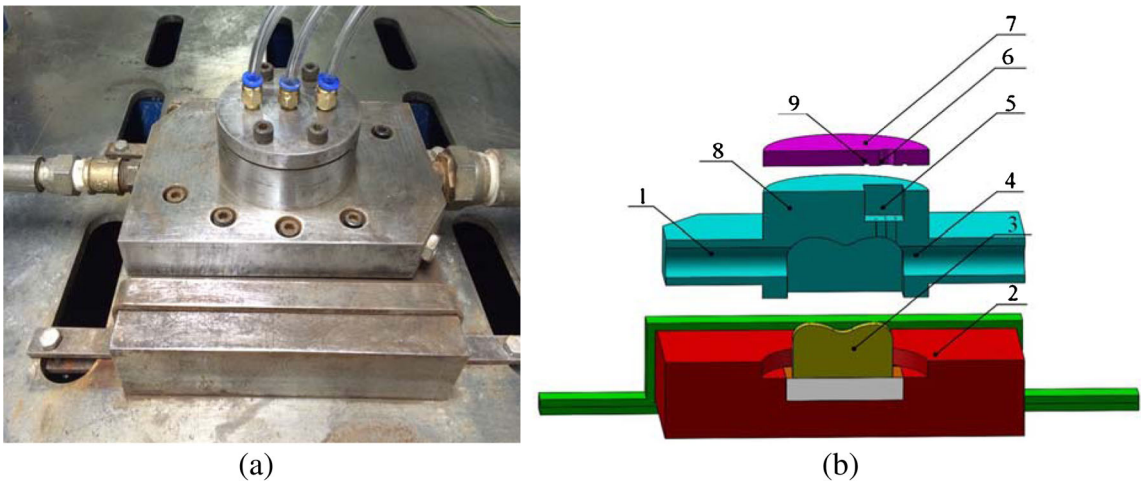

Fig. 13 GCAF experimental platform: **a** physical entity, **b** schematic diagram; *1* passage outlet, *2* constrained base entity, *3* workpiece (artificial joint), *4* passage inlet, *5* gas chamber, *6* gas inlet, *7* end cap, *8* constrained profiling modules, *9* sealing ring

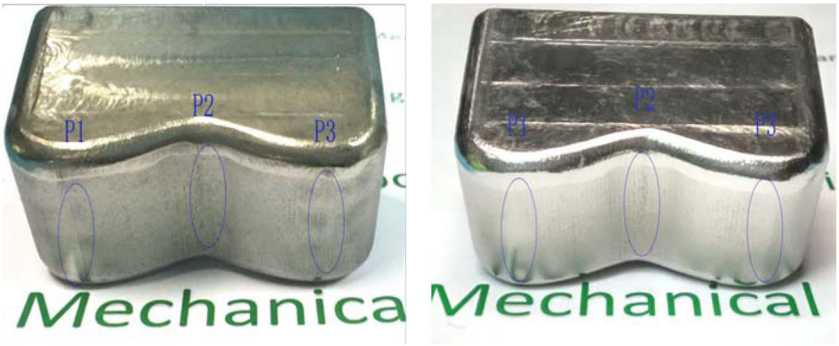

(a) (b)

Fig. 14 Processing effects of artificial joint base entity by the traditional SAF processing method: **a** before processing, **b** after 20 h processing

Considering the three-phase fluid mixing process, the incidence angle of gas phase is a key parameter. Accordingly, to study the flow field characteristics about different incidence angles of gas compensation, the corresponding profiles of velocity and dynamical pressure are shown in Figs. 11 and 12, in which the six incidence angles are selected from 0° to 115°, referring to the flow direction; the gas compensation area is front-intermediate area; the velocity of gas inlet is 10 m/s.

From the figures, it can be found that incidence angle of gas compensation has an apparent influence to flow field of GCAF, in which the intermediate-back segment takes on the best regulation effects, and the flow variation of the middle concave tends to be not remarkable. From 0° to 90°, the influence effects of incidence angle increase gradually and become weaker when the angle is larger than 90°. With respect to the dynamical pressure profile, the uniformity of front segment tends to be improved at 115°. Therefore, vertical gas injection can perform better regulation effects for the flow field of GCAF.

4 Processing experiments

4.1 GCAF experimental platform

To check the effectiveness of the proposed processing method, a GCAG processing experimental platform is developed, as shown in Fig. 13. As the key apparatus, the constrained flow passage is mainly composed of a base component, several constrained profiling modules, and a complex curved workpiece surface. A cylinder is retained at the top of constrained profiling component. A gas chamber is placed in the cylinder and sealed by an end cap. A layer of impermeable membrane is installed in the internal surface of constrained flow passage to prevent water and abrasive into the air chamber.

For the processing course, GCAF enters from the passage inlet and develops into turbulence flow because of the regulating effects of constrained flow passage. Then, the gas filled into the gas chamber whose flow quantity can be adjusted by a control valve. Concerning the three-phase fluid medium, liquid phase is water, and the density is 0.9982×10^3 kg/m^3; the solid phase is SiC particle (600# and 1200#); the medium is mixed by 90% liquid phase and 10% solid phase; the gas phase is air driven by a compressor. Workpiece is a base-entity of artificial thigh-bone joint with curved surface. GCAF is transported by a submersible pump with the flow quantity of 18 m^3/h.

4.2 Experiment results and discussion

According to the technical procedures for titanium alloy materials, the processing experiments contain two stages: rough erasing and finishing. For the first stage, the 600# SiC particles are used to erase the surface burr caused by the machining

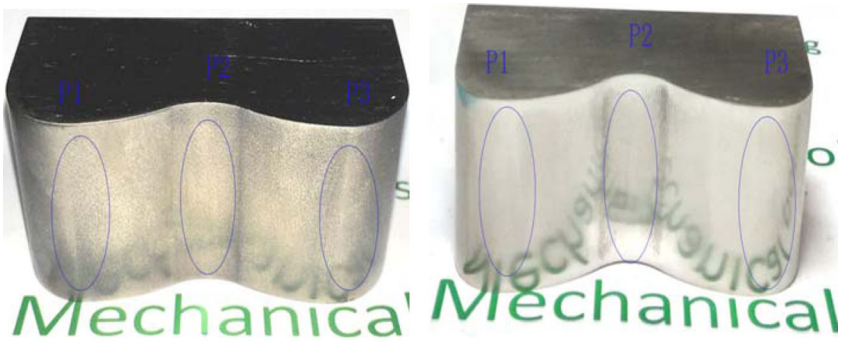

(a) (b)

Fig. 15 Processing effects of artificial joint base entity by the proposed GCAF processing method: **a** before processing, **b** after 20 h processing

operations. The second adopts the 1200# SiC particles to perform the final surface finishing. In order to obtain better surface quality, besides the regulation for gas inlet velocity, gas compensation area, and incidence angle, the flow direction requires to be changed one time per 2 h. The three roughness observation points, so-called P1, P2, and P3, are selected, with the distances of 10, 30, and 50 cm to the passage inlet, as shown in Figs. 14 and 15.

Based on the experimental platform, taking the base entities of artificial thigh-bone joints (shown in Figs. 14 and 15) as the object processed, two groups of processing experiments are performed. The first group processing experiment has no gas compensation, i.e., the traditional SAF processing method, and the other adopts the gas compensation, with the conditions of gas inlet 10 m/s, global compensation, and incidence angle 90°.

In Fig. 14, the traditional SAF processing method can decrease the surface roughness of artificial joint. However, owing to the special processing characteristics of the titanium alloy materials, it cannot perform the mirror level surface quality and not satisfy the practical requirements of artificial joints. Moreover, in the middle concave of the workpiece surface, the processing effects are worse than other regions, which accords with the numerical simulation results in Sect. 3. In Fig. 15, compared with the SAF method, the proposed method can obtain more less surface roughness, and the surface quality can reach the mirror level. Moreover, the surface quality of the middle concave segment is improved apparently.

It is well known that the surface roughness is the most important parameter for the surface quality. By a laser-based roughness measurement instrument, the roughness data of the three observation points (P1, P2, P3) are shown in Figs. 16 and 17.

According to the data in the above two figures, it can be found that the surface roughness of two groups of experiments are all decreased after 20 h processing. Regarding the same surface roughness, the second group requires less processing time, which proves that the gas compensation can increase the processing efficiency effectively. The final average surface

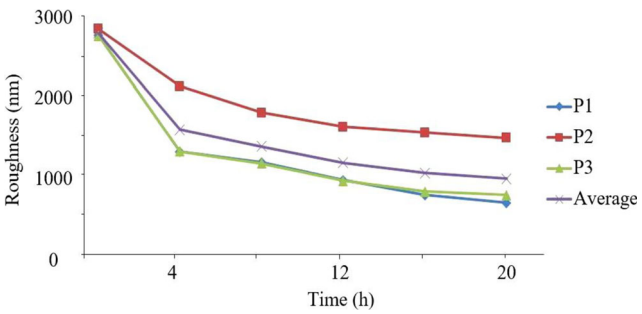

Fig. 16 Surface roughness data of the first group experiment (no gas compensation)

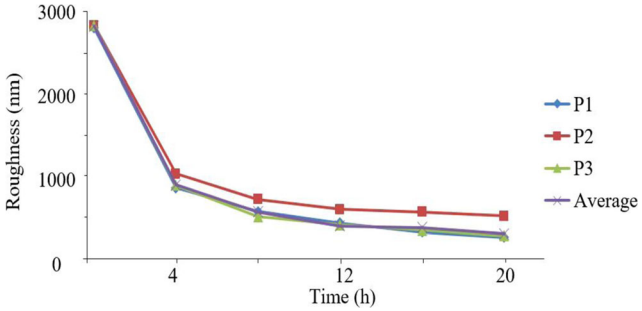

Fig. 17 Surface roughness data of the second group experiment (gas compensation)

roughness of the second group is less than one-third of that of the first group; apparently, the proposed processing method can improve the surface quality. For the roughness observation points, P1 is with the best surface quality, and P2 is the worst one. Due to the gas compensation and regular exchange of processing direction of the workpiece, the processing effects of P1 and P3 are with consistent states, while the P2 still has a certain progress effect.

Surface topography is an important technical index to assess the working performance of a processing method. Taking the finishing surface of artificial joint as the observation object, the two groups of surface topography data are by using a microscope with 500 times, as shown in Fig. 18. Similarly, the first group of experiment has no gas compensation, and the second adopts the proposed processing method. From the figure, we can find that the proposed can obtain better surface topography, and the original machining marks are obviously removed on P1 and P3. Due to the micro cutting effect of GCAF, the processed workpiece obtains a high shape accuracy, size precision, surface roughness, and surface integrity.

To obtain the detailed surface topography data of the processing surface, the 3D surface topography is acquired by a white-light interferometry system, as shown in Fig. 19. From the figures, we can refer the following regulars. (1) The two processing method can decrease the surface roughness level effectively, and the proposed GCAF method can obtain more uniform 3D topography results, especially for the back segment of workpiece surface (P3). (2) Because the gas phase enhances the turbulence intensity of the abrasive flow, the proposed method can form disorder surface texture. (3) Compared with the traditional SAF method, the proposed method can make the average topography amplitude decrease more than 50%, and the surface roughness of micro-peak and micro-valley can reach less than 50 and 10 μm, respectively. (4) For the front segment (P1), it is with the highest surface quality, but the roughness value only decrease 33%, which accords with the simulated results in Sect. 3.

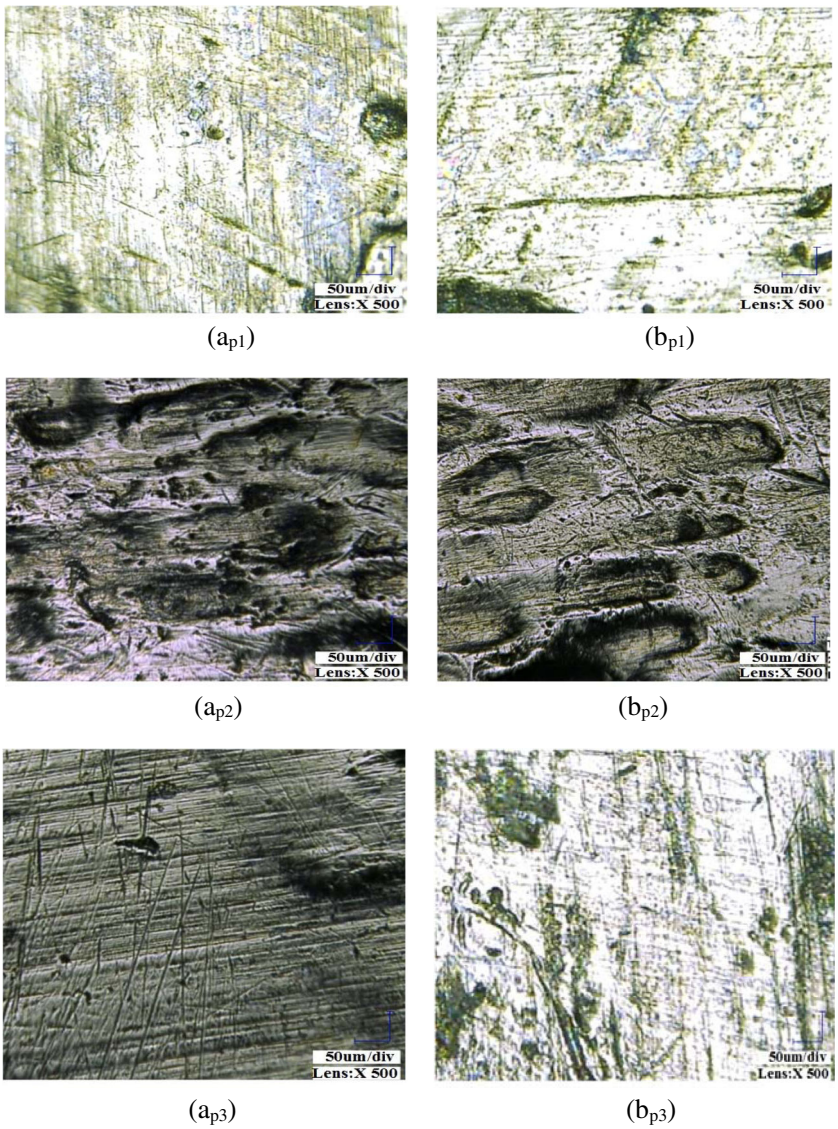

Fig. 18 Surface topography data of the two groups of processing experiments: (a_{p1}) first-group-P1, (b_{p1}) second-group-P1, (a_{p2}) first-group-P2, (b_{p2}) second-group-P2, (a_{p3}) first-group-P3, (b_{p3}) second-group-P3

5 Conclusions

As the special metal objectives, titanium alloy materials make the traditional fluid-based processing methods be subject to many difficulties. To address the matter, we propose a GCAF processing method for titanium alloy artificial joints, and the corresponding conclusions are as follows.

(1) Taking a titanium alloy thigh-bone joint as the research objective, a constrained flow passage covering the titanium alloy surface is constructed by the multiple constrained modules. A three-phase fluid mechanic model for GCAF is set up based on the realizable k-ε model and the mixture model. Numerical results show that the gas compensation can generate effective regulation effects on velocity and dynamical pressure in the front and bottom concave of the constrained passage; the global gas compensation scheme can obtain the most uniform flow field profiles, especially for the intermediate-back segment of the constrained flow passage; incidence angle of gas compensation has an apparent influence to flow field of GCAF, and the vertical gas injection can perform better regulation effects.

(2) A GCAF processing experimental platform is established, and the comparative experiments with the SAF method are performed. The experiment results show that the proposed method can obtain more less surface roughness, and the surface quality can reach the mirror level; for the same surface roughness, the proposed method requires less processing time, which proves that the gas compensation can increase the processing efficiency; the surface topography amplitude

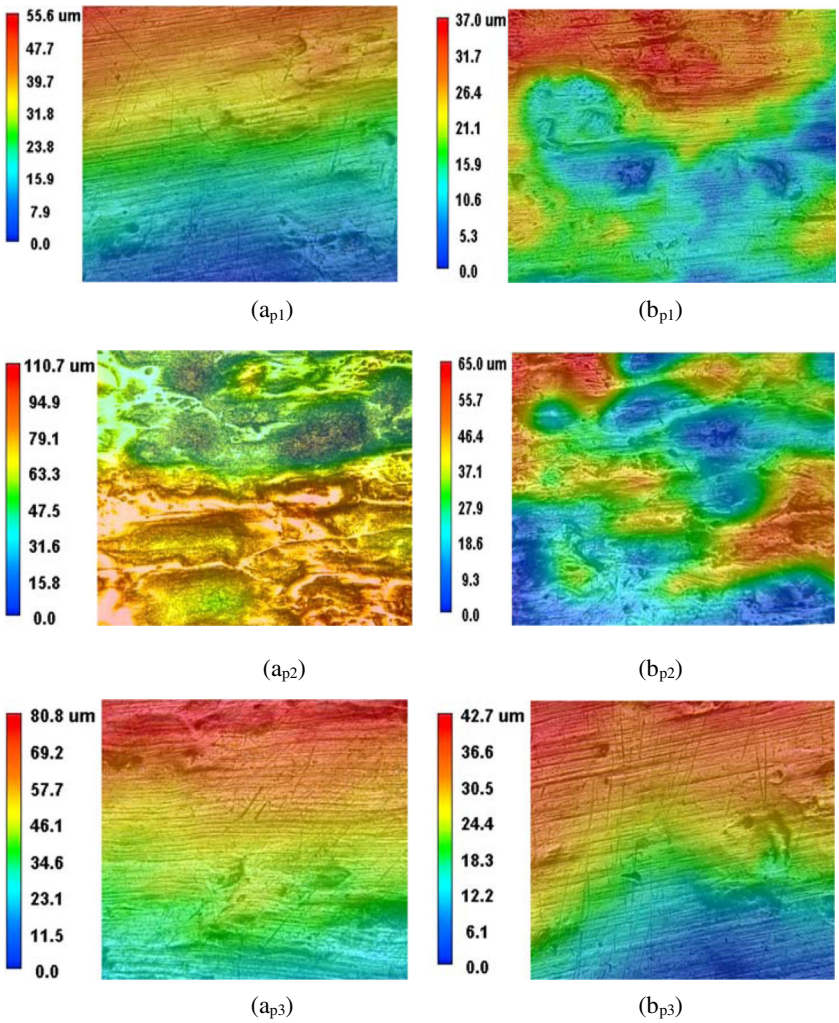

Fig. 19 3D topography data of the two groups of processing experiments: (a_{p1}) first-group-P1, (b_{p1}) second-group-P1, (a_{p2}) first-group-P2, (b_{p2}) second-group-P2, (a_{p3}) first-group-P3, (b_{p3}) second-group-P3

can decrease more than 50%, and the surface roughness of micro-peak and micro-valley can reach less than 50 and 10 μm, which prove that the method can perform better surface uniformity.

In general, the main contribution of the paper is providing a three-phase abrasive flow processing method with several gas inlets. The gas injection increases the internal energy and turbulence intensity of fluid medium, so the processing efficiency and surface quality are improved. This research not only can offer theoretical references to the three-phase fluid mechanic modeling-solving for fluid-based processing methods, but can supply direct technical supports for the optimization of abrasive flow processing. The subsequent research works will be performed on the level-set based multi-phase fluid modeling method for titanium alloy joint finishing.

Acknowledgements This work was supported in part by the Natural Science Foundation of China under Grant Nos. 51575493, 51375446; the Zhejiang Provincial Science Foundation under Grant Nos. LY15E050020, LR16E050001; the Commonweal Technology Project of Science and Technology Department of Zhejiang Province under Grant No. 2012C21093; the Visiting Scholar Foundation of the State Key Lab of Digital Manufacturing Equipment & Technology under Grant No. DMETKF2013006.

References

1. Zeng Xi, Li Jue-hui, Ji Shi-ming, Pan Ye, Hang Wei, Chen Guo-da (2017) Research on machining characteristic of double-layer elastomer in pneumatic wheel method. Int J Adv Manuf Technol (Article in Press, DOI: 10.1007/s00170-017-0226-0)
2. Wang ZW, Taskin AA, Frolich T, Braden M, Ando Y (2016) Superconductivity in Ti0.6Bi2Te3 derived from a topological insulator. Chem Mat 28(3):779–784
3. Pal VK, Choudhury SK (2008) Fabrication of texturing tool to produce array of square holes for EDM by abrasive water jet machining. Int J Adv Manuf Technol 85(9–12):2061–2071
4. Li C, Ji SM, Tan DP (2012) Study on machinability and the wall region of solid-liquid two phase softness abrasive flow. Int J Adv Manuf Technol 61(9–12):975–987
5. Wang CT, Jin ZM (2012) Wear analysis of artificial hip joint and reasoning of clinical failure diagnosis. J Med Biomech 27(4):361–368

6. He Y, Wu Y, Fu JZ, Gao Q, Qiu JJ (2016) Developments of 3D printing microfluidics and applications in chemistry and biology: a review. Electroanalysis 28(8):1658–1678
7. Zhao YQ, Liu HJ, Yang TF, Lin Z, Hu YY (2016) Study of temperature and material flow during friction spot welding of 7B04-T74 aluminum alloy. Int J Adv Manuf Technol 83(9–12):1467–1475
8. Lambiase F, Paoletti A, Di Ilio A (2016) Mechanical behaviour of friction stir spot welds of polycarbonate sheets. Int J Adv Manuf Technol 80(1–4):301–314
9. Zeng X, Ji SM, Jin MS, Tan DP, Li JH, Zeng WT (2014) Investigation on machining characteristic of pneumatic wheel based on softness consolidation abrasives. Int J Precis Eng Manuf 15(10):2031–2039
10. Ji SM, Xiao FQ, Tan DP (2010) Analytical method for softness abrasive flow field based on discrete phase model. Sci China - Technol Sci 53(10):2867–2877
11. Ji SM, Tang B, Tan DP, Gong B, Yuan QL, Pan Y (2010) Structured surface softness abrasive flow precision finish machining and its abrasive flow dynamic numerical analysis. Chinese J Mech Eng 46(15):178–184
12. Tan DP, Ji SM, Li PY, Pan XH (2010) Development of vibration style ladle slag detection method and the key technologies. Sci China - Technol Sci 53(9):2378–2387
13. Ji SM, Xiao FQ, Tan DP (2010) A new ultraprecision machining method with softness abrasive flow based on discrete phase model. Adv Mater Res 97-101:3055–3059
14. Yuan QL, Ji SM, Tan DP, Zhang L (2011) Analytical method for softness abrasive flow field based on low Reynolds k-epsilon model. Adv Mater Res 188:230–235
15. Ji SM, Zhong JQ, Tan DP, Chi YW (2012) Research of distribution and dynamic characteristic of particle group in the structural flow passage. Key Eng Mater 499:271–276
16. Zeng X, Ji SM, Jin MS, Tan DP, Ge JQ (2015) Research on dynamic characteristic of softness consolidation abrasives in machining process. Int J Adv Manuf Technol 82(5–8):1115–1125
17. Ji SM, Weng XX, Tan DP (2012) Analytical method of softness abrasive two-phase flow field based on 2D model of LSM. Acta Phys Sin 61(1):010205
18. Ji SM, Qiu Y, Cai YJ, Tan DP (2014) Research on mechanism of ultrasound enhancing and the experiment based on softness abrasive flow. Chinese J Mech Eng 50(7):84–93
19. Zhang L, Deng B, Xie Y, Zhang R, Ji SM, Wen DH (2015) Curved surface turbulence precision machining method for artificial joint complex of titanium alloy. Mater Res Innov 19(S8):55–59
20. Tan DP, Ji SM, Fu YZ (2016) An improved soft abrasive flow finishing method based on fluid collision theory. Int J Adv Manuf Technol 85(5–8):1261–1274
21. Ji SM, Huang XH, Tan DP, Tan YF (2016) Gas-liquid-solid abrasive flow polishing and its process parameter optimization. Opt Precis Eng 24(4):855–864
22. Tan DP, Zhang LB (2014) A WP-based nonlinear vibration sensing method for invisible liquid steel slag detection. Sensor Actuat B - Chem 202:1257–1269
23. Tan Da-peng, Ni Ye-sha, Zhang Li-bin (2016) Two-phase sink vortex suction mechanism and penetration dynamic characteristics in ladle teeming process. J Iron Steel Res Int (Article in Press)
24. Chen JL, Xu F, Tan DP, Shen Z, Zhang LB, Ai QL (2015) A control method for agricultural greenhouses heating based on computational fluid dynamics and energy prediction model. Appl Energ 141:106–118
25. Tan DP, Li PY, Ji YX, Wen DH, Li C (2013) SA-ANN-based slag carry-over detection method and the embedded WME platform. IEEE T Ind Electron 60(10):4702–4713
26. Tan DP, Li PY, Pan XH (2009) Application of improved HMM algorithm in slag detection system. J Iron Steel Res Int 16(1):1–6
27. Zeng X, Ji SM, Tan DP, Jin MS, Wen DH, Zhang L (2013) Softness consolidation abrasives material removal characteristic oriented to laser hardening surface. Int J Adv Manuf Technol 69(9–12):2323–2332
28. Tan DP, Ji SM, Jin MS (2013) Intelligent computer-aided instruction modeling and a method to optimize study strategies for parallel robot instruction. IEEE T Educ 56(3):268–273
29. Tan DP, Yang T, Zhao J, Ji SM (2016) Free sink vortex Ekman suction-extraction evolution mechanism. Acta Phys Sin 65(5):054701
30. Li C, Ji SM, Tan DP (2013) Multiple-loop digital control method for 400Hz inverter system based on phase feedback. IEEE T Power Electron 28(1):408–417
31. Tan DP, Li PY, Pan XH (2008) Intelligent industry monitoring network architecture UPnP based. Chinese J Electron 17(4):607–610
32. Tan Da-peng, Chen Shu-ting, Bao Guan-jun, Zhang Li-bin (2017) An embedded lightweight GUI component library and the ergonomics optimization method for industry process monitoring. Front Inform Technol Elect Eng (Article in Press, DOI: 10.1631/FITEE.1601660)
33. Castilla R, Gamez-Montero PJ, Ertürk N, Vernet A, Coussirat M, Codina E (2010) Numerical simulation of turbulent flow in the suction chamber of a gearpump using deforming mesh and mesh replacement. Int J Mech Sci 52(10):1334–1342
34. Gruber MC, Radl S, Khinast JG (2016) Effect of bubble-particle interaction models on flow predictions in three-phase bubble columns. Chem Eng Sci 146:226–243
35. Li Jun, Ji Shi-ming, Tan Da-peng (2017) Improved soft abrasive flow finishing method based on turbulent kinetic energy enhancing. Chinese J Mech Eng (Article in Press, DOI: 10.1007/s10033-017-0071-y)
36. Mei DQ, Wang H, Yao ZH, Li Y (2016) Numerical modeling and optimization of the segmented PbTe-BiTe-based thermoelectric leg. J Appl Phys 120(12):124503